Chemical Engineering Science 203 (2019) 54–67

Contents lists available at ScienceDirect

Chemical Engineering Science

journal homepage: www.elsevier.com/locate/ces

Review

Water in nanotubes: The surface effect

Mateus H. Köhler [a,b,*], José R. Bordin [c], Carolina F. de Matos [d], Marcia C. Barbosa [b]

[a] Departamento de Física, Universidade Federal de Santa Maria, 97105-900 Santa Maria, Brazil
[b] Instituto de Física, Universidade Federal do Rio Grande do Sul, 91501-970 Porto Alegre, Brazil
[c] Departamento de Física, Instituto de Física e Matemática, Universidade Federal de Pelotas, PO Box 354, 96010-900 Pelotas, Brazil
[d] Campus Caçapava do Sul, Universidade Federal do Pampa, 96570-000 Caçapava do Sul, Brazil

HIGHLIGHTS

- Nanotube functionalization offers means to achieve high water flow and selectivity.
- Fluids thermodynamics and dynamics highly affected by nanotube polarity.
- Challenges and perspectives are highlighted.

GRAPHICAL ABSTRACT

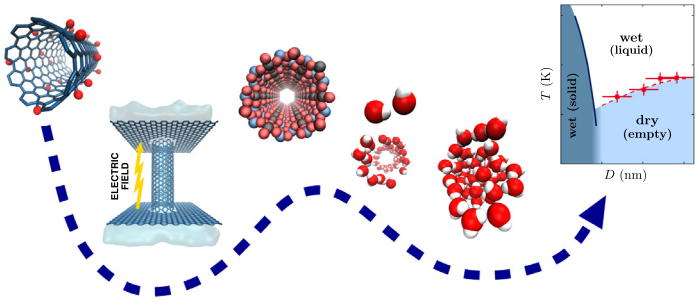

ARTICLE INFO

Article history:
Received 15 September 2018
Received in revised form 14 March 2019
Accepted 24 March 2019
Available online 26 March 2019

Keywords:
Nanotube
Water
Hydrophobic surface
Hydrophilic nanotubes

ABSTRACT

Recent advances in nanotube synthesis and functionalization have allowed for new insights into several physical-chemical aspects of nanofluidics. Processes thought possible only in theory are now attainable experimentally. This raises new questions about the distinctions between fluid behavior in bulk or under extreme confinement. Particularly, the interaction between water molecules and the nanotube wall is expected to play a major role in fluid structure and dynamics. In fact, the very definition of surface hydrophobicity is a sensitive subject, which demands further investigation. Here we present an overview of how changes in interaction and confining distances between water molecules and the nanotube wall can induce freezing, wet/dry transitions and even produce high flow rates. We suggest that the changes in water dynamics due to wall's nature (if hydrophobic or hydrophilic or mixed) indicates that polarity is the key factor for the high mobility of confined water.

Contents

* Corresponding author at: Departamento de Física, Universidade Federal de Santa Maria, 97105-900 Santa Maria, Brazil.
E-mail address: mateus.kohler@ufsm.br (M.H. Köhler).

https://doi.org/10.1016/j.ces.2019.03.062
0009-2509/

1. Introduction

Research on mass nanoscale transport through materials with nanochannels has become an emerging area – maybe one of the greatest of 21th century chemical-physics. Indeed, nanofluidics is one of the remaining territories in fluid transport with new mechanisms and phenomena yet to be discovered in spite of hydrodynamics being an established, age-old area of study.

In the past few years the activity around nanofluidics has strongly increased, with a number of groups developing creative methods to fabricate nanoscale fluidic systems (Lee et al., 2018; Setaro, 2017; Ibrahim et al., 2016). Novel experimental tools have also been engineered to probe fluid behavior in ultra-confined environments (Hassan et al., 2018; Agrawal et al., 2017; Sotthewes et al., 2017; Secchi et al., 2016). A current challenge is the design of individual fluidic channels at nanoscale, with dedicated geometrical or chemical specificities, leading to different water-wall interactions (Köhler et al., 2019, 2018).

For many applications in nanofluidic technology and almost all situations in the biological domain the behavior of interfacial water is of prime importance. The geometric constraint of a solid surface, as well as the interactions between water molecules and the substrate, lead to structural changes of water compared to its bulk counterpart.

Surfaces can be divided into two classes regarding their affinity with water. In one end of the spectrum are the hydrophilic surfaces, which possess polar groups that are capable of forming hydrogen bonds with water molecules – water–attracting. These surfaces are characterized by small or even vanishing water contact angles. In the other end of the spectrum are nonpolar, hydrophobic surfaces, which are characterized by contact angles $\theta > 90°$– water–repellent. The hydrogen-bonding network is distorted at such surfaces, resulting in a fluctuating vapor-like depletion layer with far-reaching consequences for solvation processes (Patel et al., 2012). However, in theoretical models of aqueous interface systems, it is common to use the terms hydrophilic and hydrophobic to assess different degrees of attraction modeled by Lennard-Jones type potentials, which is an approximation of genuinely polar (i.e., in the presence of partial charges) and nonpolar interactions, respectively.

Another aspect in which the confining system influences a fluid is within their hydrodynamics behavior. Over the past years it has become increasingly clear that when modeling confined systems, the no-slip boundary condition, that is, the condition of zero interfacial fluid velocity, does not necessarily hold at nanoscopic length scales (Joly, 2011; Goh and Chen, 2017; Ternes et al., 2018). In fact, the hydrodynamic boundary condition at the liquid/solid interface is of particular importance for nanofluidic applications (Bocquet and Tabeling, 2014; Majumder et al., 2005; Bocquet and Barrat, 2007) or biological nanoscale scenarios, such as the transport through membrane channels (Gomes et al., 2009; Gravelle et al., 2013). Surface slippage amplifies the flow rate for pressure driven flow, which enhances fluid transport in narrow channels.

In this respect, carbon nanotubes (CNTs) are the ultimate one-dimensional (1D) hydrophobic surfaces for water transport. Their sp^2 hybridized carbon atoms, arranged in a cylindrical honeycomb lattice, provide a smooth hydrophobic inner core which allows for uninterrupted and spontaneous passage of water molecules with very little absorption (Majumder et al., 2005). This phenomena is mainly related to the restricted space for the hydrogen bond formation inside the CNT, which aligns water molecules along the axial direction of the nanotube (Hummer et al., 2001). For these reasons, we may consider CNTs as the most promising model system for nanoconfinement studies of fluids.

Recent advances in the development of reliable methods for nanotube chemical functionalization have increased the motivation towards extending the scope of their applications. For instance, covalent modification schemes have allowed persistent alteration of the electronic properties of the nanotubes (Oytun et al., 2017; Machado et al., 2016), as well as to chemically tailor their surface properties (Bensghaier et al., 2017; Park et al., 2006), whereby new functions can be implemented that cannot otherwise be acquired by pristine nanotubes. CNTs functionalized in this way are soluble in many organic and inorganic solvents once the CNT's hydrophobic nature is changed to hydrophilic through the attachment of polar groups. The chemically functionalized CNTs can produce strong interfacial interactions with many polymers, providing CNT-based nanocomposites new properties and/or a significant improvement in existing ones (Balasubramanian and Burghard, 2005; Matos et al., 2012).

Physical functionalization, on the other hand, may be less damaging to the nanotube structure. The suspension of CNTs in the presence of polymers leads to the polymer wrapping around the CNT to form supramolecular complexes of CNTs, which alter the nanotube wall interactions and consequently their polarity. Inorganic nanoparticles (e.g., C_{60}, Ag, Au and Pt (Georgakilas et al., 2007)) can be inserted at defect sites localized at the tube's ends or sidewalls. Small biomolecules, such as proteins and short DNA chains, can also be entrapped in the inner hollow channel of nanotubes by simple adsorption, forming natural nano-test tubes (Hirsch, 2002). Also, surfactants can functionalize the CNT ends, external and internal surface with distinct goals as to control the CNT electronic structure for biocompatibility or self-assembly in mesoscale structures (Strano et al., 2003; Shim et al., 2002; Zhang et al., 2006). The combination of these materials are particularly useful in the development of hybrid channels for the use in nanotechnology and molecular scale devices.

In addition to the functionalization of hydrophobic carbon nanotubes, recent methods allowed the synthesis of structurally similar nanotubes with polar atom groups, such as boron-nitride nanotubes (BNNTs) (Wei et al., 2013). In this branch, we can also highlight the aluminophosphate ($AlPO_4$) (Gavazzoni et al., 2017), silicate (AlSi) (Zang et al., 2009), titanate (TiO_2) (Miyauchi and Tokudome, 2007) and molibdenite (MoS_2) nanotubes (Wang et al., 2016).

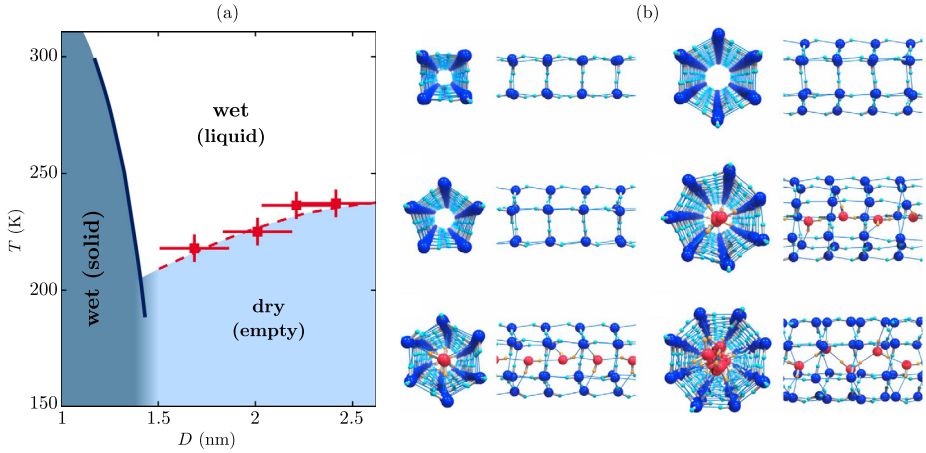

Fig. 1. (a) Schematic temperature-diameter ($T-D$) phase diagram for the water-CNT system. Solid and dashed lines represent the liquid-solid and wet-dry transition boundaries, respectively. The "wet (solid)" phase has structures referred to as ice-nanotubes. The "wet (liquid)-dry (empty)" boundary is defined as the end point of the wetting process on heating, obtained from XRD measurements (filled squares (Kyakuno et al., 2011)). (b) front view and the corresponding side view of the inherent hydrogen bond structures of six ices formed in the nanotubes. Adapted with permission from Mochizuki and Koga (2015).

The water-nanotube interaction tuning through increasing their hydrophilic or hydrophobic status is important either to achieve higher water permeation or to induce it to experience structural and dynamical transitions (Hummer et al., 2001). However, the impact of hydrophobicity over the nanopore water transport is currently under debate and may lead to significant changes in fluid organization and mobility (Kumar et al., 2005; Bordin and Barbosa, 2017; Köhler et al., 2017). Nanotubes functionalized with hydrophobic and hydrophilic sites present an opportunity to study the effect of polarity heterogeneity over confined water properties.

In this review, two aspects which impact the behavior of confined water are analyzed. First, the physical-chemical mechanisms exhibited by water confined in polar and nonpolar nanotubes are addressed and discussed in detail. Next, the structural features of the different types of confinement and its consequences to fluid mobility are presented.

2. Phase transitions induced by confinement

2.1. Solid-liquid transition

It has been extensively shown that confined or interfacial water is highly relevant to properties and functions of entire systems (e.g., ion channels (Aryal et al., 2015; Bordin et al., 2012), clay minerals (Yesilbas et al., 2018; Yesilbas and Boily, 2016), transmembrane proteins (Li et al., 2014)). Additionally, exciting new properties have emerged when water is confined in CNTs (Agrawal et al., 2017; Dalla Bernardina et al., 2016). This environment is favorable for new physical mechanisms to manifest, since the surface becomes an important ingredient in the interaction between water molecules.

Initially, the entry of water into the hydrophobic interior of a CNT may seem counterintuitive, since confinement is generally expected to decrease both water entropy and bonding. However, X-ray diffraction (Maniwa et al., 2005), neutron scattering (Kolesnikov et al., 2004) and NMR studies (Maniwa et al., 2007) verified the spontaneous water filling of the CNT's inner space at ambient conditions. The confinement is able to freeze water into crystalline solids often referred to as "ice nanotubes" (Takaiwa et al., 2008; Mochizuki and Koga, 2015; Pugliese et al., 2017) as illustrated in Fig. 1. The ice structures are characterized as stacked, ordered polygonal rings of water molecules, or equivalently as a rolled square-net sheet (Koga et al., 2000). Additionally, the number of water molecules in the ring depends on the size of the nanotube, Fig. 1(b).

This spontaneous filling, goes beyond the ice nanotubes phase. Pascal et al. (2011) found that water inside CNTs is more stable than in the bulk. The nature of the favorable confinement, however, changes dramatically with the pore diameter as it is shown in Fig. 1(a). Three stages of nanotube filling were revealed: an entropically (both rotational and translational) stabilized vapor-like phase of water for small CNTs (0.8–1.0 nm), an enthalpically stabilized ice-like phase for medium-sized CNTs (1.1–1.2 nm), and a bulk-like liquid phase for tubes larger than 1.4 nm, stabilized by the increased translational entropy as the water sampled a larger configurational space. Simulations with structureless coarse-grained water models further revealed that the observed free energies and sequence of transitions arise from the tetrahedral structure of liquid water (Pascal et al., 2011). Thus, the thermodynamics of water under confinement are intimately connected to the structure of water and its pore size commensurability.

Therefore, below the critical confinement scale (~2 nm), the theory on the depression of water's freezing point described by the continuum thermodynamics breaks down (Christenson, 2001). This was corroborated by Agrawal and collaborators (Agrawal et al., 2017). They showed that the phase behavior of water inside single and double-walled nanotubes can be monitored using the dynamic shift in the frequency of the Raman radial breathing mode (RBM). Their experiments demonstrated that the phase transitions of confined water in CNTs are extremely diameter-dependent, and freezing transitions as high as 413 K (138 °C) for 1.0 nm metallic CNTs were observed, which was close to the range of enthalpy stabilized, ice-like water as predicted by the theoretical work of Pascal et al. (2011).

The structure assumed by water and its dependence with the confining material's organization and hydrophobicity remains an open subject which requires further investigation. It is known that confined water freezes into square, pentagonal, hexagonal (I_h), and heptagonal ice nanotubes (Koga et al., 2001). The transition is either continuous (unlike any bulk substances, including bulk water) or discontinuous (despite of the fact that it is essentially in one dimension), relying on the CNT diameter or on the applied pressure (Koga et al., 2001). Spontaneous formation of octagonal ice nanotubes (Shiomi et al., 2007), ice nanotubes with hydrophobic guest molecules (Tanaka and Koga, 2005), single and multi-layered helical ice nanotubes (Noon et al., 2002; Bai et al., 2006)

have been predicted. The analysis of ice structures have suggested the existence of at least nine ice phases in the cylindrical space, including those reported by X-ray diffraction studies and by simulations (Takaiwa et al., 2008). Each ice has a structure that maximizes the number of hydrogen bonds under the cylindrical confinement. Many local maxima in the melting curve have been shown, each corresponding to the highest melting point for each ice form, with the global maximum in the melting curve located within a carbon nanotube with 1.1 nm of diameter (Takaiwa et al., 2008). In this case, each water molecule has four cooperative hydrogen bonds, which are more curved than in hexagonal ice. Other ices (for example, pentagonal, hexagonal and heptagonal nanotubes of water molecules, all with two donor and two acceptor hydrogen bonds) are formed within CNTs increasing up to 1.9 nm in diameter (Bai et al., 2006). Conversion between these ices can be achieved by increasing the pressure such that the square ice converts to pentagonal ice at about 200 MPa along 275 K isotherm (Koga et al., 2002). The versatility of ice known for bulk water seems to maintain in nanoconfinement, apparently with even more anomalies. A global picture of the temperature–diameter phase diagram of water inside CNTs is shown in Fig. 1(a).

The behavior of the phase diagram of confined water raises many questions. One of them concerns the observation that liquid water may transform into a low-dimensional ice either via a first-order phase change or without any discontinuity in thermodynamic and dynamic properties, which suggests the existence of solid-liquid critical points in this class of nanoconfined systems. In fact, the intriguing possibility of the critical point has been suggested before for other strongly confined substances (He et al., 2014; Koga and Tanaka, 2006; Bordin et al., 2014). Simulations of water confined in CNTs has provided evidence of the solid-liquid critical point (Mochizuki and Koga, 2015): macroscopic solid-liquid phase separation below a critical temperature (T_C), diverging heat capacity and isothermal compressibility at around T_C, and the loci of response function maxima above T_C.

Possible transition between two phases of supercooled liquid water has been only predicted to occur below 230 K from simulations (Palmer et al., 2014; Smallenburg et al., 2014). Such phase transition cannot be detected at a laboratory because of the so-called "no-man's land" under deeply supercooled condition, where only crystalline ices have been observed (Gallo et al., 2016). There are recent evidences that inside isolated small CNT (1.25 nm in diameter) both low and high-density liquid water states can be detected near ambient temperature and above ambient pressure (Nomura et al., 2017). In the temperature–pressure phase diagram, the low– and high–density liquid water phases have been found to be separated by an hexagonal ice nanotube phase.

Along with size effects, weak van der Waals (vdW) forces between the inner surface of the nanotube and the water molecules can be strong enough to induce phase transitions at ambient conditions. In a very recent contribution, Shayeganfar et al. (2018) modeled water molecules inside CNTs and BNNTs of various chiralities, with diameters between 0.8 and 1.2 nm. They demonstrated that the intermolecular potential of the nanotube walls exert diameter-dependent additive or subtractive vdW pressure on the solid-like water nanotube, altering the water's phase boundaries. The middle-diameter nanotubes ($\sim$ 1 nm) were found to have a major impact on the balance between molecular interactions and the vdW pressure that prompted the transition from a square water tube to an ice nanotube. The strongest interactions were found in BNNTs due to the particular atomic polarization.

The overall picture may be even more complicated than previously thought. Recently, Farimani and Aluru (2016) showed the existence of multiple phases of water when it meets a nanotube surface under atmospheric conditions. Vapor, high-density ice, and liquid water phases coexist in the region within $\sim$1 nm from the surface. A new high-density solid state ice layer (ρ = 3.9 g/cm^3) with rhombic structure coexisting adjacent to vapor and liquid water was found. The existence of multiple phases of water near an interface can explain, for example, the slip phenomena (Secchi et al., 2016), the self-filling behavior of a carbon nanotube (Naguib et al., 2004), and fast transport of water (Majumder et al., 2005).

Notably, the arrangement of the nanotube atoms must play an important role in the events taking place within the phase diagram of the confined water. A crucial question is: what does a water molecule "feel" when it enters the cavity of a nanotube? The response is usually associated with the structure of the pore itself. The smaller the nanotube, the greater its influence on the structure of the water (Köhler and da Silva, 2016). CNTs, for example, may exhibit metallic characteristics when rolled up in the armchair direction, or may be a semiconductor otherwise (Liu et al., 2013). This alone would be enough for a series of consequences on the confined fluid. Several studies have shown that water diffusion is reduced in armchair nanotubes compared with zigzag (Liu et al., 2005; Liu and Wang, 2005). In order to investigate the nanotube corrugation effect over diffusivity of confined water, Liu et al. (2008) plotted the potential energy profile of the water molecules inside the nanotube, as shown in Fig. 2. We can clearly see that the energy barrier of diffusion pathways AB in armchair nanotube is approximately half of the same zigzag pathway. It means that the water molecules will be trapped in deeper potential wells in zigzag CNTs more than in the armchair case. This result indicates why water molecules diffuse much slower in zigzag than in armchair nanotubes. Further coarse-grained simulations have confirmed the relation between flow enhancement and the nanotube's structural attractive/repulsive characteristic (Bordin et al., 2013). Additionally, the classical dynamic calculations of Wang's group indicate that in armchair CNTs water molecules diffuse along the cylindrical surface in a spiral path, while the water molecules tend to move circlewise around the central axis in zigzag CNTs. This feature was also confirmed by further quantum mechanics calculations. Another aspect is that the mobility of the water contact layer is not necessarily the same as the mobility of water central

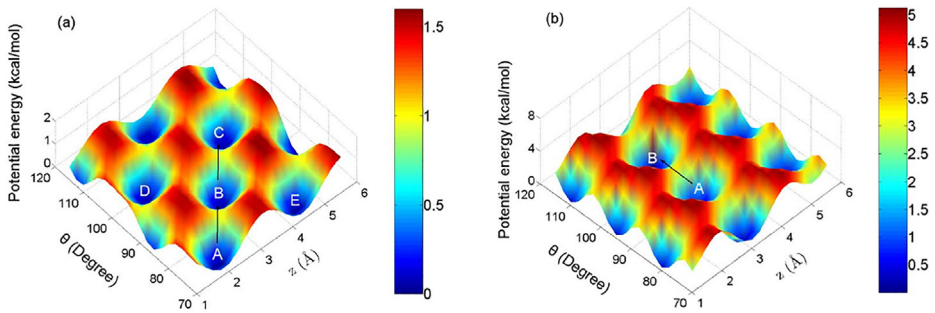

Fig. 2. 3D plots of potential energy of (a) armchair (14,14) and (b) zigzag (24,0) CNT. Adapted with permission from Liu et al. (2008).

layer (Bordin et al., 2013) probably due to the lower dielectric constant of the water at the confining wall (Fumagalli et al., 2018).

2.2. Wet-dry transition

Carbon nanotubes provide atomically smooth nanocavities, however the character of the water-surface interaction in some cases is not easily determined because the water-CNT interface exhibits hydrophobicity, which depends on the temperature T and on the nanotube diameter d (Kyakuno et al., 2011). Above a critical diameter $d_C \sim 1.4$–1.6 nm, the carbon nanotube exhibits a hydrophilic-hydrophobic transition or a wet-dry transition (WDT) at a critical temperature $T_{WD} \sim$ 220–230 K (Kyakuno et al., 2016). For $d > d_C$ this experimental study involving X-ray diffraction, optical microscopy, and differential scanning calorimetry showed that upon cooling water evaporates and then crystallizes into ice I_h outside the nanotube at T_{WD}, while upon heating the ice I_h evaporates and condenses inside the nanotube. In addition, if water is trapped inside the nanotube it freezes below T_{WD} (Kyakuno et al., 2016). Complementary to the experimental results, molecular dynamics (MD) simulations for $d > d_C$ shows that upon lowering T the hydrophobicity of these thick CNTs increases without any structural transition in the confined water, while for $d < d_C$ by decreasing the temperature the water inside these thin nanotubes exhibits a structural transition, forming an ordered ice with a well-developed hydrogen bonding network adapting to the cylindrical pore (Kyakuno et al., 2016).

The distinct structural properties observed for temperatures below and above T_{WD} can be understood as follows. Wang et al. (2008) reported a hydrophobic-hydrophilic transition upon cooling the system which indicates that the structure of interfacial water depends on temperature. At low temperatures, a considerable slowdown in molecular reorientation of the adsorbed water was also detected. At high temperatures weak hydrogen bonding might be assessed by strong orientation effects of water assemblies on hydrophobic interfaces (Scatena et al., 2001). However, at low temperatures, ice-like clusters created by strong hydrogen bonding were observed inside 2–3 nm CNT (Ohba, 2014). This anomalous structure formation is a result of unusual hydrogen bonds in CNTs.

Water behavior in interfaces can play a significant role in determining chemical reaction outcomes and physical properties. For instance, within a nanotube, the water molecules are entirely surrounded by hydrophobic/hydrophilic interfaces. In order to assess the changes in water affinity inside the CNT, Ohba and colleagues (Ohba et al., 2015) have measured the adsorption isotherms of water vapor at 300 K using a volumetric adsorption apparatus. Hydrophobic behavior of water adsorbed in channels wider than 3 nm was observed for both adsorption and desorption processes. However, water also showed hydrophilic properties in both adsorption and desorption processes in channels narrower than 1 nm. A transition between hydrophobic/hydrophilic states has been found for intermediate-sized channels in the adsorption process. Hydrophilic properties in the narrow channels for both adsorption and desorption processes were found as a result of the relatively strong water-channel interactions (10–15 kJ mol^{-1}). In the 2–3 nm channels, the water-channel interaction energy of 4–5 kJ mol^{-1} was comparable to the thermal translational energy. The cohesive water interaction was approximately 35 kJ mol^{-1}, which was larger than the others. Thus, the water affinity change in the 2–3 nm channels for the adsorption and desorption processes was attributed to weak water-channel interactions and strong, cohesive interactions.

When we think of water confined in nanotubes, the first thing that comes to mind are perfectly cylindrical nanotubes. However, nanotubes may undergo changes in their geometrical structure. Radial deformation can appear under external mechanical stress (Yao et al., 2008), electric fields (Shtogun and Woods, 2009) or in metal contacts (Perebeinos and Tersoff, 2014). Andreev et al. (2005) have explored the relationship between the mechanical properties of such channels and their interaction with water. They showed that increasing the CNT flexibility leads to an increase in their apparent hydrophobic character, while the presence of water inside the channel makes them more resistant to radial collapse, which is an important result for computational nanofluidics in rigid nanochannels. They also found that flexibility impedes water transport across the nanotube by increasing the free-energy barriers. Mendonça and collaborators showed that the tube's deformation suppresses the observed melting for the (9,9) nanotube (Mendonça et al., 2019). Conversely, the presence of water inside the nanotube affects the qualitative nature of the energy profile for radial collapse of the nanotube; in other words, the confined water affects the nanotube's mechanical properties. These results suggest a cooperative mechanism between water and nanotubes in which the behavior of water inside polar and nonpolar channels might rely strongly on the precise interatomic interactions between water and the channel.

The idea that the hydrophobicity-flexibility-related phenomena plays a very important role in water transport was confirmed by Tao et al. (2018) when they found a boost of ~20% in the water flux through flexible CNTs when compared with rigid nanotubes. This indicates that transport of water through nanotubes is related to hydrophobicity by the slippage phenomena, and this wettability effect becomes significant as the nanopore's size decreases. They also conjectured that the large slipping in the hydrophobic surface results from the relatively low water density, short residence time and small friction forces.

Briefly stated, at nanometric sizes below 2 nm, the intuitive idea that confinement shifts the water solid–liquid transition to lower temperature fails. Below these critical diameters the melting temperature depends on the nanotube's size and chirality. To add more complexity to the system, at the nanoscale the water-nanotube interaction can be either hydrophobic or hydrophilic (dry or wet) depending on the temperature and size of the confining geometry. By lowering the temperature, the water-wall interface exhibits hydrophobic-hydrophilic transitions. Similar transitions are observed as the confining size is decreased.

The polar/nonpolar (hydrophilic/hydrophobic) character of the nanotube is fundamental for understanding the properties of confined water. The key aspect is the presence or absence of long electrostatic interactions between the nanotube surface and the water molecules. While long range interactions are absent for hydrophobic surfaces, they are quite relevant and directly impact the liquid organization for the hydrophilic. The wet-dry transition is the ultimate consequence of this interaction. As we will see next, the extent of the polarity effect over the water dynamics is also remarkable.

3. Nanoconfined water flow

3.1. Slippage and flow rate in nanotubes

The classical pressure-driven flow inside a tube is described by the Hagen– Poiseuille (HP) equation (Calabrò et al., 2013; Mattia and Calabrò, 2012), which predicts a parabolic profile for the fluid's velocity inside a cylinder. This hydrodynamic framework that in principle could be used to describe the flow of water inside a nanotube, breaks down at the sub-nanometer confinement of water (Guo et al., 2015). This is consistent with the experimental flow of water confined in nanotubes with diameters smaller than 0.7 nm (Holt et al., 2006; Thomas and McGaughey, 2009). The

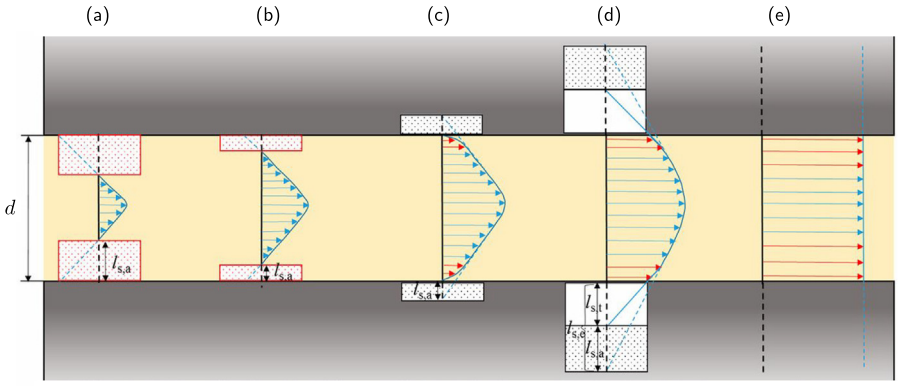

Fig. 3. Schematic representation of slip length inside nanopores. From (a) to (e), the strength of the water-wall attraction decreases and the contact angle increases (from hydrophilic to hydrophobic nanotube). (a) and (b) Apparent slip with a negative slip length, where the water-wall attraction is larger than the water intermolecular attraction. Red squares are the regions with high viscosity at which the water molecules keep static relative to the walls. (c) Apparent slip with a positive slip length, where the water-wall attraction equals the water intermolecular attraction. Red arrows are the regions with low viscosity. (d) and (e) Apparent and true slip with both positive slip lengths, where the water-wall attraction is smaller than the water intermolecular attraction. Adapted with permission from Wu et al. (2017). (For interpretation of the references to colour in this figure legend, the reader is referred to the web version of this article.)

experimental observation is 2–5 orders of magnitude larger than the value predicted by the continuum HP equations (Kannam et al., 2013). One of the ingredients responsible for the failure at the continuum HP equations is the assumption that the liquid adheres to the nanotube wall, the *no-slip* boundary condition. The zero velocity at the wall provides reliable results for macro-scale flow, but contradicts the experimental (Majumder et al., 2005; Holt et al., 2006) and theoretical (Ternes et al., 2018) evidences at the nanoscale.

In order to circumvent *no-slip* failure, the boundary condition is replaced by the linear Navier condition that preserves the shear stress at the wall (Calabrò, 2017):

$$-\lambda \frac{\partial u}{\partial x}(r = R) = u(r = R) \tag{1}$$

where $u(r = R)$ describes the velocity as a function of the distance r from the tube axis to the tube radius R (velocity profile), and λ is usually referred to as the slip length. The flow rate ($\dot{m}$) is then obtained by integrating the velocity profile $u(r)$ along the tube. The case of $\lambda = 0$ yields *no-slip*, whereas larger slip lengths flattens the velocity profile until it becomes linear, as can be seen in Fig. 3. The increase of λ is highly dictated by the coupling between the liquid and the confining material: high slippage occurs when the fluid adherence to the surface is very low (Joly, 2011) (hydrophobic nanotubes) while small slippage is associated with hydrophilic nanotubes (Peng Lee et al., 2012).

Using the *no-slip* condition in the HP equations the flow rate $\dot{m}_{HP}$ across the nanotube becomes (Borg and Reese, 2017)

$$\dot{m}_{HP} = \frac{\pi d^4 \rho \Delta P}{128 \mu l} \tag{2}$$

where d is the nanotube diameter, ρ is the fluid density, ΔP is the overall applied pressure drop, μ is the fluid viscosity and l is the nanotube length.

There are alternative solutions for the slip length calculation. For instance, the slip length is inversely proportional to a friction coefficient, which defines the liquid–solid interface friction (Schoch et al., 2008). Therefore, both the slip length and the friction coefficient are metrics used in simulations and experiments to assess water flow rates inside nanotubes. The divergence between the classical prediction, $\dot{m}_{HP}$ (*no-slip* flow), and the observed flow rate, $\dot{m}$, is calculated through the flow enhancement factor ϵ:

$$\epsilon = \frac{\dot{m}}{\dot{m}_{HP}}. \tag{3}$$

The divergence between the measured and the *no-slip* flow can be related to the different molecular and non-continuum flow behavior when water is highly confined ($d < 2$ nm). The slippage phenomena, the molecular ordering, and the nonlocal viscosity are some of the parameters that affect flow enhancement (Calabrò, 2017). Even with adjustments for fluid slip (Eq. (3)), the HP equation still does not operate well for $d < 2$ nm, as it fails to capture these crucial non-continuum phenomena (Holland et al., 2015). Simulations with more elaborated slip boundary conditions also provide flow predictions smaller than the experimental observations. Borg and Reese (2017) suggested that part of the difference is due to the large uncertainties of the experimental results when compared with the simulations. Then, in order to reconcile these results, Wu et al. (2017) employed the effective slip concept based in experiments and simulations on the physical mechanisms of nanoconfined water flow. The effective slip was defined as the linear sum of true slip (depending on the surface wettability) and an apparent slip (caused by a spatial variation of the confined water viscosity). The water flow predicted by Wu and his colleagues was as far a $10^{-1} - 10^{7}$ times that calculated by the *no-slip* HP equation depending on the surface wettability and nanopore dimension, and it is consistent with experiments and simulations.

Therefore, flow and boundary conditions of water confined in nanotubes are determined by the intermolecular attractions between water and the nanopore walls (Hummer et al., 2001; Thomas and McGaughey, 2009). Nevertheless, the essential physics underlying nanoconfined water flow and how it correlates with the changes in intermolecular forces remains to be fully elucidated. Recent advances in experimental techniques such as drop/bubble probe atomic force microscope (AFM) and surface forces apparatus (SFA) have provided useful insights into the intermolecular forces associated with confined water (Xie et al., 2017). Additionally, new experimental setups for the visualization of flow profiles at the solid/liquid interface have been applied to quantify the slippage phenomena (Secchi et al., 2016; Schäffel et al., 2016). The coupling between these experimental measurements and accurate molecular simulations can be used to further expand our understanding on the water-water and water-nanopore interactions at the molecular level.

3.2. From hydrophobic to hydrophilic nanotubes: controlling water flow

In their seminal work, Hummer et al. (2001) found that a minute reduction in the tube wall and water attraction dramatically affects

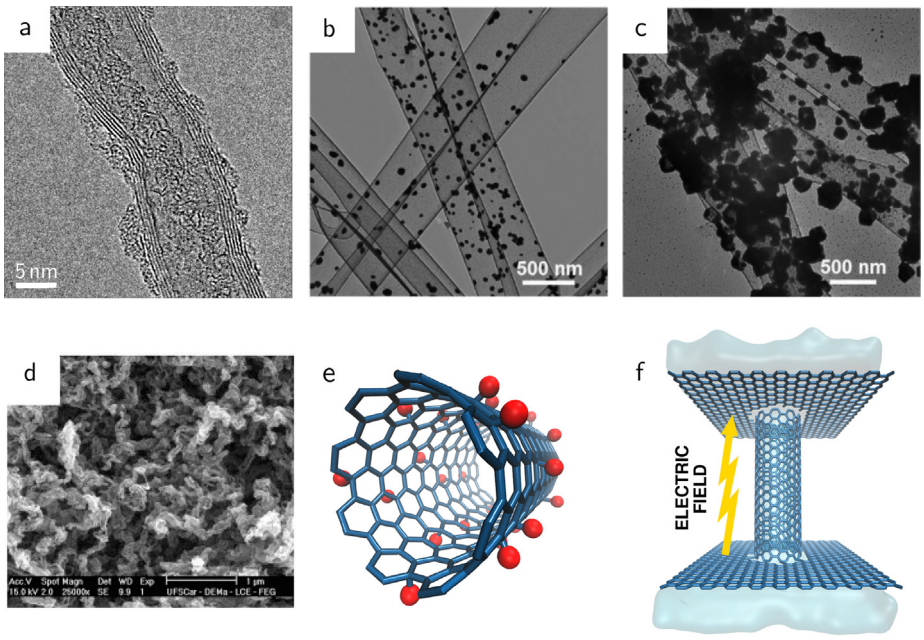

Fig. 4. (a) Transmission electron microscopy (TEM) image of SiC coated CNT irradiated with 70 keV kinetic energy Ar ions, adapted with permission from Roy et al. (2015). TEM images of CNT having their (b) innerwall and (c) outerwall modified with Pt nanospheres and nanocubes, respectively. Adapted with permission from Qu et al. (2006). (d) Scanning electron microscopy (SEM) images of oxygen plasma functionalization of CNT. Adapted with permission from Lobo et al. (2012). Schematic representation of (e) oxygenated and (f) charged CNT for molecular dynamics simulations of water conduction.

the pore hydration, leading to sharp, two-state transitions between empty and filled states on a nanosecond timescale. Further analysis of the simulation results of Hummer's group shows that water molecules inside and outside the nanotube are in thermodynamic equilibrium (Noy et al., 2007). This observation illustrates one of the most important phenomena associated with nanofluidic systems: confining a liquid inside a nanotube channel can actually lower its free energy. Further simulations by the same group (Waghe et al., 2002) showed that the filling's equilibrium is very sensitive to water-nanotube interaction parameters: a 40% reduction in surface-water attraction results in the emptying of the nanotube cavity.

Biomimetic asymmetric – hydrophilic-hydrophobic – nanochannels have recently attracted increasing attention from researchers. The asymmetric wettability designed to control the wetting behavior of aqueous media induces water motion through the tube. The idea is inspired by the stenocara beetle living in the Namib Desert: it utilizes a hydrophobic surface with a random array of hydrophilic bumps on its back to collect pure water. Scientists have extended this idea to nanochannels via chemical modification, which allows for the channel to be partially hydrophobic and hydrophilic (Roy et al., 2015; Duan et al., 2013; Hou et al., 2010; Qu et al., 2006). Fig. 4 presents a schematic illustration of functionalized nanotubes.

Chen et al. (2011) have studied nanotubes asymmetrically modified with hydrophilic groups (carboxyl, $-COOH$) at one tip and hydrophobic groups (trifluoromethyl, $-CF_3$) at the other. Reduced water density on the hydrophobic sides is observed – except for the narrowest (6,6) tube, due to single-file water dipole orientation change. In general, these functionalized nanotubes have demonstrated relatively high energy barriers for ion permeation at their tips. In this case, the tip functionalization offers the possibility of stable water conduction with ionic exclusion as a reward.

In order to understand the impact of non-uniform hydrophilic functionalization on the water mobility, Striolo (2007) studied the water diffusion through oxygenated CNTs. In this case, distribution of hydrophilic groups was not restricted to a specific end of the tube. The work reports zero diffusion for low hydration, while Fickian diffusion appears for sufficiently large hydration levels. The findings are explained in terms of two collective motion mechanisms: the "cluster-breakage" and "cluster-libration". The cluster-breakage mechanism is related to longer water displacements than the cluster-libration, but deactivates as water fills the carbon nanotube. Remarkably, the diffusion of water molecules can be highly reduced by charge discontinuity introduced by the oxygen atoms on the nanotube wall.

Then, Zuo et al. (2010) questioned the impact of a directional functionalization in water mobility. They studied the single-file water transport through a biomimic water channel consisting of a (6,6) CNT with different types of external point charges distributed along the tube axis in order to cause dipole orientation. It was demonstrated that, as in the aquaporins (de Groot and Grubmüller, 2005), asymmetrically positioned charges interfere with the unidirectional water flow in the nanotube. Thermal fluctuation in bulk water competes with charge affinity to steer the water transport, resulting in nonmonotonic flow with intermittent reversal of transport direction. Additional energetic analysis suggested that the water–water interaction, determined by the dipole orientation configuration, significantly influences both the hydrogen bonding network and the transport rate. Design of efficient functional nanofluidic devices is, therefore, intimately dependent on the charge distribution along the nanotube, with the possibility of tuning water flux by modulating the dipole orientation and the polarity of the functional groups attached to the nanotube.

The boundary condition is indeed a critical issue in nanoscaled systems. Small changes in surface–water interaction can lead to extreme consequences to the fluid transport. In addition to understanding how hydrophilic groups distribution affects the water dynamics, another relevant question is how the specific hydrophilic energy interaction influences the water. Melillo and collaborators (Melillo et al., 2011) addressed this point through MD simulations. They have found the existence of a narrow transition region in which water occupancy and flux through the nanotube increases dramatically with increasing interaction strength, as shown in Fig. 5(a). Interestingly, this transition region coincides with water contact angles close to 90° on graphene, hinting at a

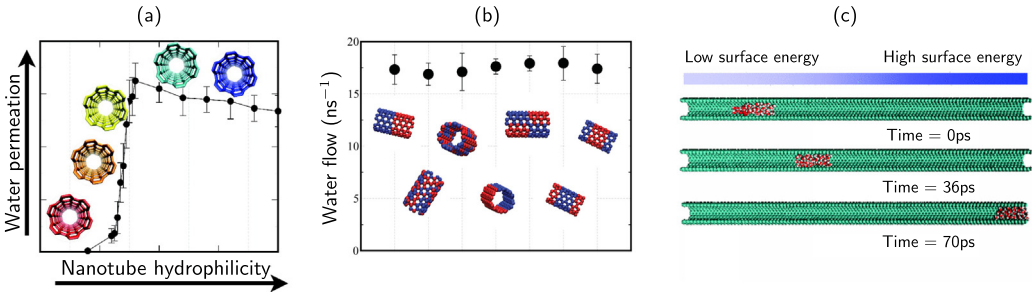

Fig. 5. Molecular dynamics results for (a) water permeation and (b) water flow in nanotubes with tunable hydrophobicity, adapted with permission from Melillo et al. (2011) and Moskowitz et al. (2014), respectively. (c) Water movement for hydrophobicity gradient in nanotubes. Adapted with permission from Kou et al. (2012).

fundamental link between nanotube wetting characteristics and water transport.

The variation of the atomic distribution and interaction strength in the nanopore leads to distinct changes in the water mobility. The combination of both effects is related to anomalous behaviors of confined water. By varying fractions f of hydrophilic atoms arranged on a honeycomb lattice to mimic functionalized nanotubes, Moskowitz et al. (2014) studied a system in which the hydrophobicity was changed both by varying the position of the sites and their interaction with water. The authors found that water occupancy vary nonlinearly as a function of f, and a small fraction of hydrophilic atoms ($f \sim 0.4$) can induce spontaneous and continuous filling of the nanotube. Markedly, the average number of water molecules inside the channel and water flux through the nanotube are less sensitive to the specific arrangement than to the fraction of hydrophilic atoms, as shown in Fig. 5(b). It is intriguing, however, that when located in the tube entrance, the hydrophobic atoms can have some role lowering the filling rate (Ramazani and Ebrahimi, 2016).

Controlling water flow into cavities as narrow as nanotubes is in fact a challenge. However, the correct polarity tuning could help with this task. For instance, Kou et al. (2012) have demonstrated unidirectional motion of water molecules through nanotubes created only by a nonzero surface energy gradient, as depicted in Fig. 5(c). They have found that water moves along the direction of increasing surface energy, and that higher surface energy gradient promotes higher transport efficiency. With a wavelike feature, the hydrogen bond network has been demonstrated to play an important role in the dynamic acceleration process. This is a very important result for reactions such as the hydrogen evolution of water (Misra et al., 2009) and the recovering of mechanical energy into electrical current through water movement inside nanotubes (Ghosh et al., 2003).

Another way to see the effects of confining water was employed by Xu et al. (2016). They investigated single-walled nanotubes as model nanochannels, changing the strength of water-nanotube attraction in order to mimic hydrophobic/hydrophilic nanotubes. They found threshold values for drying states, wetting–drying transition states, and stably wetting states: as the strength of water-channel attractions increases, first water flow increases rapidly to then decrease gradually. Surprisingly, they observed a maximal flow when empty states are present in the inner nanotube, which is unexpected since in this situation the wired hydrogen-bonding network (prerequisite for high water permeability (Hummer et al., 2001; Bordin et al., 2012, 2014)) is broken. This indicates that appropriate empty-filling (drying-wetting) switching can promote water permeation. Xu's group also found a negative correlation between the flipping frequency of single-file water and the water-channel attraction, mostly dictated by the axial dipole moment of inner water molecules.

The effort of designing high-flux nanochannels have permeated nanofluidic science throughout the last decades, and still represents a huge challenge regarding the physical-chemical understanding of such systems. Furthermore, we have observed from both experiments and simulations that classical behaviors (expected from bulk) are constantly frustrated when water is confined in nanotubes, and the channel polarity seems to be an important ingredient, dictating the anomalies most of the time. In the Stokes–Einstein theory, for instance, the mobility of a fluid is constrained to the relation: $D \propto T\eta^{-1}$. However, we have demonstrated that when water is confined in narrow hydrophobic nanotubes, the Stokes–Einstein relation is broken in order to establish a steady diffusivity (Köhler et al., 2017), similarly to what is found in supercooled liquids (Tarjus, 1995). Markedly, this effect is mainly dictated by the hydrogen bonding network and the structure assumed by water molecules inside such environment.

The combination of hydrophobicity and temperature induces distinct dynamic behaviors of confined water. We showed that the temperature is a critical parameter for water mobility inside hydrophobic and hydrophilic nanotubes (Köhler and Bordin, 2018). Our results indicate that the increase in water density leads to higher structuration for all samples at the cost of mobility. Particularly for higher temperatures a different diffusion of water was found when confined in hydrophilic nanotubes, compared with hydrophobic pores. Similarly, water diffusion dependence on temperature is distinct for different nanotube sizes. This variation is also accompanied by changes in the water organization inside each nanotube.

The nature of the material composing the nanotube surface is often determinant for their polarity character. Nanotubes composed of boron nitride (BN), silicon carbide (SiC) and others surface heterogeneities, such as $AlPO_4$ nanotubes, have been investigated for nanofluidic applications. Interestingly, non-equilibrium (NEMD) simulations of water transport across membranes made of armchair (8,8) BNNTs and armchair (8,8) CNTs showed water fluxes very close to each other (Suk et al., 2008), suggesting similarities in the friction coefficients of both nanotubes. This result is in contrast with the majority of the works devoted to the subject. For instance, Brog and Reese have shown that CNTs have the highest flow enhancement factor compared with BNNTs and SiC nanotubes (Borg and Reese, 2017). Secchi et al. (2016) showed experimentally a surface slippage in CNTs not observed in BNNTs with similar diameters, with water being transported more efficiently in the former. The disagreement may lie within two main aspects. The first is the computational method used in the work of Suk et al. (2008). Kannam et al. (2017) have pointed deficiencies in NEMD simulations of water inside nanotubes, mainly related with difficulties in accessing the velocity profile and the limitations of the model size. An alternative method involves equilibrium (EMD) simulations, which have more reliable results for velocity

measurements. The second aspect is related to the electronic structure of the nanotubes. For instance, Thomas et al. (2014) indicated that the rapid transport of water in hydrophobic nanopores has its roots in the smooth energy landscape, which gives rise to a frictionless surface and a depletion layer near the nanotube-water interface. Indeed, recent evidences of Wei and Luo (2018) point toward a significantly smoother potential energy landscape inside zigzag CNTs compared with zigzag BNNTs, and thus smaller water friction coefficients. This is a result of the lack of partial charges in CNTs which hinders the electrostatic interaction with water molecules. Markedly, the partial charges bearing armchair BNNTs also lead to electrostatic interactions with water. However, the atomic arrangement in these pores does not create local potential energy traps, and thus the friction coefficient is smaller than in its zigzag counterparts.

This local traps are more likely to occur inside nanotubes with heterogeneous molecular distribution, that is, with hydrophilic and hydrophobic molecular sites. Though their smooth inner surface is an important ingredient for the water conduction, CNTs, BNNTs and similar nanotubes of specific diameters are difficult to obtain experimentally. Moreover, the partial metallic nature of CNTs restrict spectroscopic investigations of confined water. In contrast, synthetic imogolites, i.e., aluminosilicate nanotubes with monodispersed diameters (Mukherjee et al., 2007), allow for different chemical groups at the tube surface while maintaining a well-defined geometry (Amara et al., 2015; Maillet et al., 2011), a very important aspect for nanofluidics. Therefore, synthetic imogolites provide a promising route for producing tunable, 1D-confining systems. Their heterogeneous surface with rough energy profiles provide means for the local structuration of water molecules through a varied hydrogen bond network. In a recent contribution, Liao and his colleagues (Liao et al., 2018) have used infrared spectroscopy to investigate water confinement in self-sustaining imogolite thin films. Two types of synthetic imogolites were investigated: pristine imogolite with a hydrophilic inner surface covered with Si−OH groups and hybrid imogolite with a hydrophobic inner surface covered with $Si-CH_3$ groups. A red-shift in the O−H stretching band indicates the formation of strong H bonds along the hydrophilic tube, while a small contribution around 3,633 cm^{-1} is indicative of weakly hydrogen-bonded water molecules inside the hydrophobic pores ($Si-CH_3$ terminations). This weakly hydrogen-bonded water was also observed in small hydrophobic CNTs (Hummer et al., 2001), suggesting the formation of *single-file* water with larger intermolecular distances inside imogolite nanotubes than in CNT.

Aluminophosphate nanotubes also provide well-defined heterogeneous geometry, allowing for the study of water permeance with high accuracy. Alabarse and collaborators (Alabarse et al., 2012) have prepared $AlPO_4$ crystals of high quality to allow the ordering of confined water to be determined precisely using X-ray diffraction. They found distinct and anomalous freezing of water inside these nanostructures: while the pore surface induces orientational order of water in contact with it, water does not crystallize at temperatures as low as 173 K. In a recent work, our group have also found anomalous diffusion of water molecules confined in $AlPO_4$ nanotubes, with mobility increasing with density (Gavazzoni et al., 2017). The results indicate that this phenomena is related to the increase of the number of neighbors leading to the formation of interstitial water and distorted H-bonds. Interestingly, Zang et al. (2009) have shown different diffusion of water through AlSi nanotubes in comparison with others hydrogen-bonding liquids (methanol and ethanol), which highlights the peculiarities of water transport through nanopores.

The vast literature analyzing water confined in nanotubes indicates that there are distinct behaviors of water flowing through hydrophobic, hydrophilic and heterogeneous nanotubes. Although computational simulations, especially MD simulations, have afforded most of these results, there is still room to better describe, and therefore understand such systems. For instance, the polarizability can have a significant effect on simulations of water models. Kumar et al. (2015) have shown that the inclusion of polarizability quantitatively affects the nature of hydrogen bonding of the water models inside CNTs. Markedly, they found that, as in the case of bulk water (Barrat and McDonald, 1990), the inclusion of flexible bonds and angles does not improve the results for the dynamic behavior and sometimes leads to results that are worse than those obtained for the SPC/E model. On the other hand, flexible water models can provide improved predictions of surface tension (Yuet and Blankschtein, 2010). MD simulations of ionic solutions through CNTs and near polarizable surfaces also evidenced the dependence of diverse transport and structural features on the various atomic models employed, including polarizability (Beu, 2010; Bordin et al., 2016). In fact, recent research has suggested that several factors such as bond flexibility, long-range electrostatic interactions, and certain simulation parameters, such as Lennard-Jones (LJ) cutoff distance and simulation time, may play an important role in determining the simulated water properties. This shows how careful one must be with the details involved in a simulation of nanofluidic systems. Nevertheless, we have shown that with the proper simulational framework it is possible to access information that otherwise would never be available, making computational simulations an important tool in studying and designing new nanofluidic devices.

3.3. External electric field effects on water transport

As a water molecule passes through a nanochannel the energy barrier could serve as a significant physical quantity through which water's transport behavior can be determined. It is very likely for a water molecule to cross the inner channel of a nanotube with a lower energy barrier, rather than a higher energy barrier condition. Adjusting the energy barrier can thus control the transport behavior of water molecules.

An external electrical field may strongly influence the behavior of dipolar liquids in nanoenvironments and affect the solid−liquid interface tension (Vaitheeswaran et al., 2004). Consequently, it becomes attractive to control nanofluidic behavior through electrical fields. In this way, Liu et al. (2008) reported several mechanisms governing the pressure-driven infiltration of water into a CNT with external charges applied, demonstrating that specific arrangements of charges, exactly as the hydrophilic sites in the Moskowitz's work (Moskowitz et al., 2014), can control the effective infiltration pressure. They used MD simulations to show that the applied charges can increase the effective degree of hydrophobicity, which leads to an improved adjustability of energy absorption efficiency.

Moreover, Gong et al. (2007) found that charges can be an excellent controllable pumping source in driving water molecules' faster transport through nanochannels. Following Gong's work, Su and Guo (2011) presented the effect of an electric field on the transport of a *single-file* of water molecules through a short carbon nanotube. When an external electrical field is applied to a water-filled CNT the water inside it is forced to escape from the pore as the external work reduces the effective potential energy. According to Bonthuis et al. (2010,), however, both works fall into the same trap: the cutoff scheme implemented in their GROMACS simulations. The problem lies in the approximation method used to handle electrostatic interactions within GROMACS that (with the wrong cutoff scheme) can lead to spurious results. This can be the case, for instance, of the work of Joseph and Aluru (2008a), that found an electro-osmosis of water inside CNTs in the absence of free charges. This finding is in disagreement with the Onsagers reciprocal theorem, which states that an externally applied pres-

sure drop cannot cause a steady electric current. In fact, simulations on nanofluidic systems are often intricate, laborious, and inspires extra care to describe correctly all the atomic interactions, under penalty of reaching the wrong conclusions on the flow and structure of the confined fluid. For extensive, clarifying reviews on how the computational methods can impairs the simulation results the reader is referred to (Wong-ekkabut and Karttunen, 2016; Merz and Shirts, 2018).

Theoretical and numerical studies to understand the intrinsic mechanisms of the escape behavior of water under external electric fields have been carried by Li et al. (2016). They have found that the cumulative probability of water escaping from the nanotube exhibits a Maxwell-Boltzmann distribution, allowing for the evaluation of the energy barrier for water spillage. Through statistical analysis, they related a blocking temperature (required for water to escape from the nanotube) and a frictional energy barrier with the dynamic escape behavior.

Other important phenomena affecting the flow rate inside a nanotube are the resistance along the nanotube and the resistance to flow at its entrance. Recently, Abbasi and Karimian (2016) investigated the effect of electric charging of CNT on these two phenomena. Charge magnitudes between zero to 1.0 *e*/atom were applied along different lengths of nanotubes, and they concluded that the electric charging can be used to manipulate these two phenomena and therefore effectively control the rate of water flow in a nanotube.

As a polar substance water is not only susceptible to the electrical field magnitude, but also to the electrical interference frequency outside the channel. Biological channels, for instance, are actually exposed to vibrational electrical signals due to metabolism, and a tiny signal may bring significant responses in nanoscaled systems (Gong et al., 2008). By performing MD simulations to investigate water permeation through a CNT with electrical interference Kou et al. (2014) found that the water net flux across the nanochannel is greatly affected by the external field, with the maximal net flux occurring at a frequency of 16,670 GHz. They attributed the above phenomena to the breakage of hydrogen bonds as the electrical interference frequency approaches to the inherent resonant frequency of hydrogen bonds. Additionally, Jianlong et al. (2015) have also found an unexpectedly high water net flux by approaching a vibrational charge to the nanochannel, unlike the fixed charge system, where the static charge is expected to attract the negatively charged oxygen in water, immobilizing the motion of water molecules (Li et al., 2007). Again, the success for the vibration charge-induced movement of water molecules lies in the disruption of the hydrogen bond network inside the nanochannel, in contrast with the strong water−water interaction that eventually induces a *single-file* chain of the confined water.

In fact, by applying pulsed electrical fields with frequencies ranging from microwave to ultraviolet, Zhou et al. (2017) showed that the motion mechanism (characterizing the diffusion) of water confined in narrow CNT is changed from Fickian to ballistic and *single-file* diffusion.

Consistent with previous studies, Zhang et al. (2018) used BNNTs with different charge distributions as a model to investigate water transport through functionalized nanotubes. As in the case of CNTs, the transport of water molecules was found to be highly influenced by the charge regulation in the terminal of BNNTs. It was showed that water transport would be enhanced depending on the directional effect of the applied electric field and the enlargement of the channel.

The use of external electric fields to control the water flux through hydrophobic, hydrophilic and functionalized nanotubes is therefore a very promising branch of nanofluidics, with several applications such as in selective membranes, nano-sieves and osmotically-driven electrical current nano-devices (Vuković et al., 2014; Li et al., 2013).

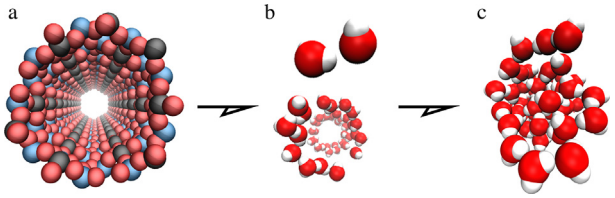

Fig. 6. Front view (axial projection) of the (a) aluminophosphate nanotube (i.e., rough surface energy profile) and the structure assumed by the confined water at (b) low and (c) high density regime, both exhibiting string-like, helicoidal arrangement, as studied in the work of Gavazzoni et al. (2017). Red, black, white and blue spheres represent, respectively, the oxygen, aluminum, hydrogen and phosphorus atoms. (For interpretation of the references to colour in this figure legend, the reader is referred to the web version of this article.)

3.4. Water packing at different nanotube interfaces

The structure assumed by water molecules inside hydrophobic nanotubes has been extensively studied, but when confined in hydrophilic or functionalized nanopores water also presents intriguing properties. Inside such environments, surface interaction and available space may cause raised or lowered melting points in water: while cubic ice is found in 4.2 nm diameter hydrophilic silica tubes at 232 K (Christenson, 2001), in narrow (1.5 nm diameter) silica pore water does not freeze above 130 K (Liu et al., 2013).

Nanotubes that are not as smooth as CNTs have also been studied as confining environments. Aluminophosphate, silicate and MoS_2 nanotubes are some examples, with polar and nonpolar sites coexisting within the cavity. Particularly, the high valence of the Al atoms in the aluminophosphate pore may lead to an irregular distribution of water near the wall. Alabarse et al. (2012) have found an ubiquitous unfreezable water layer at the center of the $AlPO_4$ nanopore. X-ray diffraction, Raman spectroscopy, and molecular simulations were used to show that this layer has a rigid (i.e., glassy) liquid-like structure, but can also exhibit orientational order. Additionally, they found suppressed crystallization at the nanotube interface as the number of hydrogen bonds becomes insufficient.

Simulations have shown that inside $AlPO_4$ nanotubes the water structure is controlled by the heterogeneity of the pore's surface (Gavazzoni et al., 2017), with the water molecules located preferentially next to the oxygen atoms in the nanotube; consequently, at very low densities, water forms helicoidal structures in string-like arrangement, as shown in Fig. 6. In fact, water molecules ordered in helix with long-range order in the axial direction were observed also inside CNTs (Liu and Wang, 2005). The tetrahedron structure of water molecules in O—H bonding and interactions of the water molecules with the π electrons along the C—C bond direction was mentioned as a possible cause of the helix structuring of water molecules.

By investigating the transport properties of hydrogen-bonding liquids (water, methanol, and ethanol) through a single-walled aluminosilicate nanotube, Zang et al. (2009) found a segregation between mixtures of water and methanol. Remarkably, they found the water molecules also located closer to the tube wall and the alcohol molecules localized near the center of the nanotube. Apparently, the heterogeneity of the nanopore "attracts" more the water than the other liquids which, as we have shown, have several consequences over their dynamic and thermodynamic properties.

In a recent contribution we have analyzed the structural behavior of high and low density water inside hydrophobic and hydrophilic nanotubes with distinct radii (Köhler et al., 2018). The fluid structure was found to be highly affected by the water-nanotube interaction, and the influence is enhanced by the increase in

density. Accordingly, the water mobility is lowered by the packing of water molecules at the nanotube interface, specially for the lower densities. In fact, the combination of a high density water layer and a depletion region is characteristic of water in a CNT interface (Cicero et al., 2008). In this case, however, water is "disconnected" from the surface so that flow rate is maintained and even increased (Köhler and da Silva, 2016). Joseph and Aluru (2008b) have attributed this phenomena to the water orientations and the hydrogen bonding at the nanotube interface. For nanotubes with the same smooth wall structure but with hydrophilic silicon atoms instead of carbon, the flow is reduced because it does not have "free" OH bonds pointing to the wall, as in CNTs, that would reduce the number of hydrogen bonds in the depletion layer. On the other hand, rough nanotubes induce water to exhibit strong hydrogen-bonding network, which in turn impairs the water flow (Joseph and Aluru, 2008b; Xu et al., 2011).

In summary, both the dynamics and the structure of confined water are governed by the permeation process, with roots in the lowering of the free energy and an optimized hydrogen bond network, and also by the slip boundary conditions, which guarantees the emergence of the so-called super-flux of water in nanotubes. In both cases, however, since the hydrogen bond network plays a relevant role, hydrophobicity and polarizability definitively affect the final result.

4. Applications of nanofluidics through functionalized nanotubes

The advent of nanotechnology allowed us to explore and understand the physics behind this new scale of hydrodynamics - the nanofluidics. Then, these systems became a desirable strategy for producing energy and reducing our impact on the planet, which at first seems straightforward, but in actuality conceals many subtleties and unexpected properties. Following are some possible technological applications that make use of functionalized nanotubes to induce water movement, collecting impurities and converting mechanical energy into electrical current.

4.1. Desalination

Nanotube-based membrane performances often rely on its processing and fabrication methods. It has been shown that *biotin* and *streptavidin* attachment onto the functionalized CNT membranes reduced ion transport by 5–15 times (Hinds et al., 2004). Such functionalized membranes work as gatekeeper controlled chemical separators or as ion-channel mimetic sensor. Holt et al. (2006) have incorporated silicon nitride (Si_3N_4) between the nanotubes' spaces to inhibit water flow between the nanotube gaps and create stress to stimulate water flow through the tube. The water flux was increased by more than threefold over the *no-slip* hydrodynamic flow, and presented enhanced ion selectivity compared to regular multi-walled CNT membranes. Additionally, such membrane engineering can provide high selectivity with low energy consumption.

Recently, Lee and his group (Lee et al., 2015) have used densified outer-wall CNT membranes to deliver a water purification capacity of 30,000 $L/m^2 \cdot h$ at 1 bar, which is almost two orders of magnitude greater than that attainable using traditional polymer membranes. Yang et al. (2013) have also demonstrated functionalized nanotubes to exhibit ultrahigh specific adsorption capacity for salt (exceeding 400% by weight) that is two orders of magnitude higher than that found in the current state-of-the-art activated carbon-based water treatment systems (Porada et al., 2012).

Nanopore functionalization eventually modifies the water-wall interaction, leading to new and improved water transport capability. This is particularly important for desalination processes where the water molecules would be attracted to the inner tube instead of ions. Some experimental setups and computational studies of water desalination using functionalized nanotubess are shown in Fig. 7.

4.2. Pollutant removal

As for desalination, functionalization is often a precondition for nanotube based water purification. Pristine CNTs often aggregate, which significantly decreases water flux and pollutant rejection capacities of the nanotubes. Additionally, in the fabrication process the nanotube surface is generally contaminated with metal catalysts, impurities and physical heterogeneities (Mauter and Elimelech, 2008). Functionalization can add positive ($-NH_3^+$), negative ($-COO^-$, sulfonic acids) and hydrophobic (aromatic rings) groups on the CNT surface (Goh et al., 2013). These make CNT membranes selective for particular pollutant retention and increase water influx through the nanotube hole.

Functionalized nanotube membranes have shown good water permeability, mechanical and thermal stability, fouling resistance, pollutant degradation and self-cleaning functions (Lee et al., 2015; Yang et al., 2013). Tip-functionalized CNTs have selective functional groups on the nanotube ends and the core functionalized CNTs have functionalities at the sidewall or interior core. Both types demonstrated increased water flux and selective pollutant rejection. Majumder and Corry (2011) have found that progressive hydrophilic modification in the nanopore walls can significantly affect the water influx, with consequences for nanofluidic devices.

Functionalization also decreases energy consumption through increased permeability and physical adjustability (Goh et al., 2013). CNT membranes can be decorated with various metallic nanoparticles, polymers, and biomolecules which have attractive membrane properties and thus broadening functionalized CNT applications – as in molecular sieves.

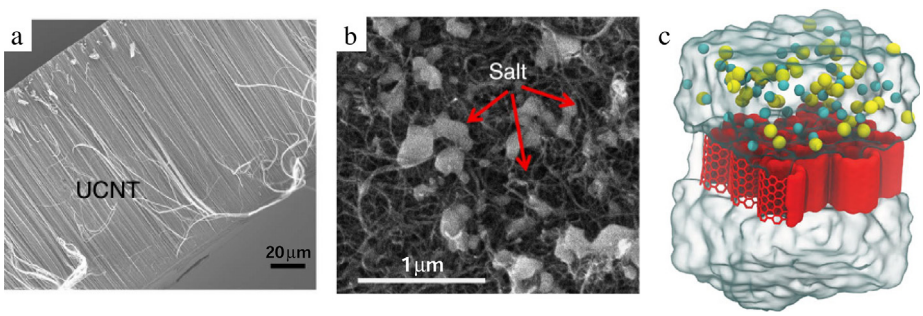

Fig. 7. (a) Cross-sectional SEM image of plasma-modified CNT membranes. (b) Same membranes after the adsorption reaches saturation. Adapted with permission from Yang et al. (2013). (c) Angled view of simulation with CNT membranes for water-ion separation. Adapted with permission from Thomas and Corry (2015).

4.3. Energy conversion

Whether the fast flow (mechanical energy) of water or polar liquids in functionalized nanocavities can be converted into electrical energy is an extremely interesting subject. The potential electric current and voltage generation in graphitic materials immersed in flowing liquids was first predicted theoretically by Král and Shapiro (2001) for metallic carbon nanotubes. Since then, many experiments have reported the voltage generation phenomena. The main driving mechanism was found to be the direct scattering of free carriers by the fluctuating Coulombic fields of the flowing molecules and ions in the liquid. Ghosh et al. (2003) reported experimentally an induced voltage of 2.7 mV for pure water flowing at 1.8 mm/s outside single-walled (SW) CNT bundles. The addition of ions (1.2 M HCl solution) has lead to fourfold induced voltage. A significant dependence of the induced voltage on the flow velocity suggested that the fast flow of water (and other liquids) along the hydrophobic surface is the key component of the energy harvesting through the graphitic nanofluidics. Liu et al. (2007) have shown that multiwalled CNT vertically aligned along the flow direction produced ~30 mV in aqueous solution of NaCl (1 M) at a flow velocity of 0.5 mm/s. Again, nonlinear voltage-velocity response was observed.

Notably, experiments have demonstrated that tuning the polarity of the nanopore by decorating its surface or applying electric fields along the tube axis leads to enhanced voltage generation and improved conversion efficiency. Lee et al. (2011) have shown that voltage generated for semiconducting nanotubes was three times greater than that for metallic nanotubes, and that the pore polarity is a crucial ingredient in the energy generation through nanofluidics. Recently, Kim et al. (2016) have generated networks and carbonization between individualized SWCNTs by an optimized plasmonic heating process using a halogen lamp to improve electrical properties for flow-induced energy harvesting. The electrical sheet resistance of carbonized CNTs was decreased to 2.71 kΩ, 2.5 times smaller than pristine CNT, leading the carbonized-CNTs to present a generated voltage 9.5 times and a current 23.5 times than that of pristine CNTs.

Siria et al. (2013) have fabricated a hierarchical nanofluidic device made of BNNT, thus a hydrophilic membrane with almost the same atomic arrangement than the carbon atoms in the hydrophobic CNT membrane. They found very large, osmotically induced electric currents generated by salinity gradients, exceeding by two orders of magnitude their pressure-driven counterpart. This phenomena originates in the high surface charge carried by the nanotubes internal surface in water at large pH, and suggests the BNNT membranes as good candidates for osmotic power harvesting under salinity gradients.

As we have seen, controlling the pore polarity have several consequences to the water thermodynamics and dynamics through nanotubes. On the other hand, all of these results bring up the amazing possibilities that nanopore functionalization can add to nanofluidic devices.

5. Challenges and perspectives

We have discussed how molecular arrangement dictates water diffusion in nanotubes. It starts with *single-file*, one-dimensional clusters of hydrogen-bonded water molecules diffusing in a highly coordinated way (ballistic diffusion) inside narrow hydrophobic nanotubes (Hummer et al., 2001). We have also seen ice formations, as ice nanotubes, helixes and a range of other ice structures inside functionalized nanotubes (Melillo et al., 2011; Won and Aluru, 2008).

The main question, however, lies in the experimental confirmation of these results. Despite the efforts, this task has been proven tricky and particularly challenging. Consequently, most of the facts regarding the nature of water diffusion in nanopores at a molecular scale have been almost solely acquired by computational studies with scarce experimental works. One example is the determination of the water flow rate inside nanotubes.

Despite the hydrodynamics divergence at sub-nanometer confinement, probing experimentally the fluid flow through nanotubes offers huge difficulties and practical obstacles. Inventive experiments have been used to overcome this challenge. Secchi et al. (2016), for instance, have mapped the velocity profile of water in individual nanotubes by introducing polystyrene nanoparticles into the permeating water reservoir. By doing this, they have assessed the displacement of the tracers as water jets emerging from the CNTs and then accurately determined the water flow rates. Measuring flow rate inside nanotubes is a complicated task since mass flow through a single CNT is found to be as low as 10−15L/s (Michaelides, 2016).

In a recent contribution, Hassan et al. (2018) reported the first direct experimental evidence of stratified water diffusion in CNTs. They used NMR diffusion−relaxation ($D-T_2$) and relaxation (T_1-T_2) spectroscopy in order to experimentally resolve the distribution of the self-diffusion coefficient of water inside single- and double-walled CNTs. While in SWCNT, the ($D-T_2$) NMR spectra exhibited the characteristic shape of a uniform water diffusion, in DWCNT a nonuniform diffusion was found: a second water component was observed, which was assigned to an axial water component with values four times that of bulk water at $T = 285$ K.

The experimentalists have also been dealing with uncertainties coming from the technical challenges of fabricating well-controlled nanoscale structures. This is not particularly helpful to the experimental validation of theoretical results. For example, vertically aligned CNT membranes often exhibit either non-uniform nanochannels and inconsistently low porosity due to blockage of the nanopores (Striolo et al., 2016; Majumder et al., 2008).

The acquiring of nanotubes with well-controlled distribution, radii and shape is essential to unlock their potential applications. Growth of CNTs via structure-controllable pathways, higher synthetic efficiency, and remarkable purity have been produced with significant improvements throughout several technologies (Hsiao and Lin, 2017; Ahmad et al., 2015; Sanchez-Valencia et al., 2014). These nanotubes are mainly produced through physical-mixing of CNTs with desired matrices. However, the well-controlled growth of high-density CNTs at selected positions or desired substrates is still a challenge and requires additional research.

Schweiger et al. (2015) have used chemical vapor deposition (CVD) with iron catalyst particles on quartz substrates to create nanotubes with reliable and reproducible diameter distributions that correlated directly with the catalyst particle size distributions. Remarkably, by changing the reduction time it was possible to reproducibly shift the average SWCNT diameter from 1.5 (±0.3) to 1.2 (±0.2) nm while maintaining a nanotube density of 5–6 SWCNT/μm.

Nanopores with more complicated atomic arrangement such as metal oxide nanotubes have also been synthesized. Amara et al. (2015) have obtained hybrid single-walled imogolite nanotubes with diameter-controlled hydrophobic nanopores varying from 1.8 to 2.4 nm. A combination of infrared spectroscopy, cryo-TEM observations, and X-ray scattering measurements have shown that, in solution, the water density inside methylated nanotubes is decreased by a factor of 3 compared to the bulk value with spontaneous confinement of bromopropanol, which introduces possibilities for water decontamination through these nanopores.

Despite the hindrances, nanofluidics through functionalized polar and nonpolar nanotubes is a flourishing territory that offers

gold rush opportunities. Controlling the water flow in these nanopores is therefore not just possible, but necessary to yield highly efficient nanofluidic devices with a branch of applications, such as in desalination processing, contaminant selectivity, and energy conversion. Just as the water's structure is the key parameter affecting their mobility – and the polarity plays an important role in the structuration of water inside nanopores – the design of well-controlled functionalized nanotubes and the accuracy in measuring water flow inside these pores are preconditions for the large scale application of nanofluidics. With some challenges to overcome, the general picture is that we have experienced large technological advancements in this field in the last decade and that much more is about to come.

Declaration of Interest statement

The authors declare no conflict of interests.

Acknowledgements

This study was financed in part by the Coordenação de Aperfeiçoamento de Pessoal de Nível Superior (CAPES), Finance Code 001, Conselho Nacional de Desenvolvimento Científico e Tecnológico (CNPq), INCT-FCx, and Fundação de Amparo à Pesquisa do Estado do Rio Grande do Sul (FAPERGS).

References

Abbasi, H.R., Karimian, S.M.H., 2016. J. Mol. Liq. 224, 165–170.
Agrawal, K.V., Shimizu, S., Drahushuk, L.W., Kilcoyne, D., Strano, M.S., 2017. Nat. Nanotechnol. 12, 267–273.
Ahmad, M., Anguita, J.V., Stolojan, V., Corless, T., Chen, J.-S., Carey, J.D., Silva, S.R.P., 2015. Adv. Funct. Mater. 25, 4419–4429.
Alabarse, F.G., Haines, J., Cambon, O., Levelut, C., Bourgogne, D., Haidoux, A., Granier, D., Coasne, B., 2012. Phys. Rev. Lett. 109, 035701.
Amara, M.S., Paineau, E., Rouzière, S., Guiose, B., Krapf, M.-E.M., Taché, O., Launois, P., Thill, A., 2015. Chem. Mater. 27, 1488–1494.
Andreev, S., Reichman, D., Hummer, G., 2005. J. Chem. Phys. 123, 194502.
Aryal, P., Sansom, M.S.P., Tucker, S.J., 2015. J. Mol. Biol. 427, 121–130.
Bai, J., Wang, J., Zeng, X.C., 2006. Proc. Natl. Acad. Sci. USA 103, 19664–19667.
Balasubramanian, K., Burghard, M., 2005. Small 1, 180–192.
Barrat, J.-L., McDonald, I.R., 1990. Mol. Phys. 70, 535–539.
Bensghaier, A., Lau Truong, S., Seydou, M., Lamouri, A., Leroy, E., Micusik, M., Forro, K., Beji, M., Pinson, J., Omastova, M., Chehimi, M.M., 2017. Langmuir 33, 6677–6690.
Beu, T.A., 2010. J. Chem. Phys. 132, 164513.
Bocquet, L., Barrat, J.-L., 2007. Soft Matter 3, 685–693.
Bocquet, L., Tabeling, P., 2014. Lab Chip 14, 3143–3158.
Bonthuis, D.J., Horinek, D., Bocquet, L., Netz, R.R., 2010. Langmuir 26, 12614–12625.
Bonthuis, D.J., Falk, K., Kaplan, C.N., Horinek, D., Berker, A.N., Bocquet, L., Netz, R.R., 2010. Phys. Rev. Lett. 105, 209401.
Bordin, J.R., Barbosa, M.C., 2017. Phys. A 467, 137–147.
Bordin, J.R., de Oliveira, A.B., Diehl, A., Barbosa, M.C., 2012. J. Chem. Phys. 137, 084504.
Bordin, J.R., Diehl, A., Barbosa, M.C., Levin, Y., 2012. Phys. Rev. E 85, 031914.
Bordin, J.R., Diehl, A., Barbosa, M.C., 2013. J. Phys. Chem. B 117, 7047–7056.
Bordin, J.R., Andrade Jr., J.S., Diehl, A., Barbosa, M.C., 2014. J. Chem. Phys. 140, 194504.
Bordin, J.R., Krott, L.B., Barbosa, M.C., 2014. J. Phys. Chem. C 118, 9497–9506.
Bordin, J.R., Podgornik, R., Holm, C., 2016. Euro. Phys. J. ST. 225, 1693–1705.
Borg, M.K., Reese, J.M., 2017. MRS Bull. 42, 294–299.
Calabrò, F., 2017. MRS Bull. 42, 289–293.
Calabrò, F., Lee, K.P., Mattia, D., 2013. Appl. Mathem. Lett. 26, 991–994.
Chen, Q., Meng, L., Li, Q., Wang, D., Guo, W., Shuai, Z., Jiang, L., 2011. Small 7, 2225–2231.
Christenson, H.K., 2001. J. Phys.:Condens. Matter 13, 95–133.
Cicero, G., Grossman, J.C., Schwegler, E., Gygi, F., Galli, G., 2008. J. Am. Chem. Soc. 130, 1871–1878.
Dalla Bernardina, S., Paineau, E., Brubach, J.-B., Judeinstein, P., Rouzière, S., Launois, P., Roy, P., 2016. J. Am. Chem. Soc. 138, 10437–10443.
de Groot, B.L., Grubmüller, H., 2005. Curr. Opin. Struct. Biol. 15, 176–183.
Duan, R., Xia, F., Jiang, L., 2013. ACS Nano 7, 8344–8349.
Farimani, A.B., Aluru, N.R., 2016. J. Phys. Chem. C 120, 23763–23771.
Fumagalli, L., Esfandiar, A., Fabregas, R., Hu, P., Ares, S., Janardanan, A., Yang, Q., Radha, B., Taniguchi, T., Watanabe, K., Gomila, G., Nooselov, K.S., Geim, A.K., 2018. Science 360, 1339–1342.
Gallo, P., Amann-Winkel, K., Angell, C.A., Anisimov, M.A., Caupin, F., Chakravarty, C., Lascaris, E., Loerting, T., Panagiotopoulos, A.Z., Russo, J., Sellberg, J.A., Stanley, H. E., Tanaka, H., Vega, C., Xu, L., Pettersson, L.G.M., 2016. Chem. Rev. 116, 7463–7500.
Gavazzoni, C., Giovambattista, N., Netz, P.A., Barbosa, M.C., 2017. J. Chem. Phys. 146, 234509.
Georgakilas, V., Gournis, D., Tzitzios, V., Pasquato, L., Guldi, D.M., Prato, M., 2007. J. Mater. Chem. 17, 2679–2694.
Ghosh, S., Sood, A.K., Kumar, N., 2003. Science 299, 1042–1044.
Goh, K., Chen, Y., 2017. Nano Today 14, 13–15.
Goh, P.S., Ismail, A.F., Ng, B.C., 2013. Desalination 308, 2–14.
Gomes, D., Agasse, A., Thiebaud, P., Delrot, S., Geros, H., Chaumont, F., 2009. Biochim. Biophys. Acta 1788, 1213–1228.
Gong, X., Li, J., Lu, H., Wan, R., Li, J., Hu, J., Fang, H.A., 2007. Nat. Nanotechnol. 2, 709–712.
Gong, X., Li, J., Zhang, H., Wan, R., Lu, H., Wang, S., Fang, H., 2008. Phys. Rev. Lett. 101, 257801.
Gravelle, S., Joly, L., Detcheverry, F., Ybert, C., Cottin-Bizonne, C., Bocquet, L., 2013. Proc. Natl. Acad. Sci. USA 110, 16367–16372.
Guo, S., Meshot, E.R., Kuykendall, T., Cabrini, S., Fornasiero, F., 2015. Adv. Mater. 27, 5726–5737.
Hassan, J., Diamantopoulos, G., Gkoura, L., Karagianni, M., Alhassan, S., Kumar, S.V., Katsiotis, M.S., Karagiannis, T., Fardis, M., Panopoulos, N., Kim, H.J., Beazi-Katsioti, M., Papavassiliou, G., 2018. J. Phys. Chem. C 122, 10600–10606.
He, Y., Li, H., Jiang, Y., Li, X., Bian, X., 2014. Sci. Rep. 4, 3635.
Hinds, B.J., Chopra, N., Rantell, T., Andrews, R., Gavalas, V., Bachas, L.G., 2004. Science 303, 62–65.
Hirsch, A., 2002. Angew. Chem. 41, 1853–1859.
Holland, D.M., Lockerby, D.A., Borg, M.K., Nicholls, W.D., Reese, J.M., 2015. Microfluid. Nanofluid. 18, 461–474.
Holt, J.K., Park, H.G., Wang, Y., Stadermann, M., Artyukhin, A.B., Grigoropoulos, C.P., Noy, A., Bakajin, O., 2006. Science 312, 1034–1037.
Hou, X., Yang, F., Li, L., Song, Y., Jiang, L., Zhu, D., 2010. J. Am. Chem. Soc. 132, 11736–11742.
Hsiao, C.-H., Lin, J.-H., 2017. Carbon 124, 637–641.
Hummer, G., Rasaiah, J.C., Noworyta, J.P., 2001. Nature 414, 188–190.
Ibrahim, I., Gemming, T., Weber, W.M., Mikolajick, T., Liu, Z., Rümmeli, M.H., 2016. ACS Nano 10, 7248–7266.
Jianlong, K., Jun, Y., Hangjun, L., Bo, Z., Aifen, L., Zhixue, S., Jianguang, Z., Yunzhang, F., Fengmin, W., Jintu, F., 2015. Angew. Chem. 127, 2381–2385.
Joly, L., 2011. J. Chem. Phys. 135, 214705.
Joseph, S., Aluru, N.R., 2008a. Phys. Rev. Lett. 101, 064502.
Joseph, S., Aluru, N.R., 2008b. Nano Lett. 8, 452–458.
Kannam, S.K., Todd, B.D., Hansen, J.S., Daivis, Peter J., 2013. J. Chem. Phys. 138, 094701.
Kannam, S.K., Daivis, P.J., Todd, B.D., 2017. MRS Bull. 42, 283–288.
Kim, J., Lee, J., Kim, S., Jung, W., 2016. ACS Appl. Mater. Interfaces 8, 29877–29882.
Koga, K., Tanaka, H., 2006. J. Chem. Phys. 124, 131103.
Koga, K., Parra, R.D., Tanaka, H., Zeng, X.C., 2000. J. Chem. Phys. 113, 5037–5040.
Koga, K., Gao, G.T., Tanaka, H., Zeng, X.C., 2001. Nature 412, 802–805.
Koga, K., Gao, G.T., Tanaka, H., Zeng, X.C., 2002. Phys. A 314, 462–469.
Köhler, M.H., Bordin, J.R., 2018. J. Phys. Chem. C 122, 6684–6690.
Köhler, M.H., da Silva, L.B., 2016. Chem. Phys. Lett. 645, 38–41.
Köhler, M.H., Bordin, J.R., da Silva, L.B., Barbosa, M.C., 2017. Phys. Chem. Chem. Phys. 19, 12921–12927.
Köhler, M.H., Bordin, J.R., da Silva, L.B., Barbosa, M.C., 2018. Phys. A 490, 331–337.
Köhler, M.H., Bordin, J.R., Barbosa, M.C., 2018. J. Chem. Phys. 148, 222804.
Köhler, M.H., Bordin, J.R., Barbosa, M.C., 2019. J. Mol. Liq. 277, 516–521.
Kolesnikov, A., Zanotti, J.-M., Loong, C.-K., Thiyagarajan, P., Moravsky, A., Loutfy, R., Burnham, C., 2004. Phys. Rev. Lett. 93, 035503.
Kou, J., Mei, M., Lu, H., Wu, F., Fan, J., 2012. Phys. Rev. E 85, 056301.
Kou, J., Lu, H., Wu, F., Fan, J., Yao, J., 2014. Nano Lett. 14, 4931–4936.
Král, P., Shapiro, M., 2001. Phys. Rev. Lett. 86, 131–134.
Kumar, P., Buldyrev, S.V., Starr, Francis F.W., Giovambattista, N., Stanley, H.E., 2005. Phys. Rev. E 72, 051503.
Kumar, H., Dasgupta, C., Maiti, P.K., 2015. RSC Adv. 5, 1893–1901.
Kyakuno, H., Matsuda, K., Yahiro, H., Inami, Y., Fukuoka, T., Miyata, Y., Yanagi, K., Maniwa, Y., Kataura, H., Saito, T., Yumura, M., Iijima, S., 2011. J. Chem. Phys. 134, 244501.
Kyakuno, H., Fukasawa, M., Ichimura, R., Matsuda, K., Nakai, Y., Miyata, Y., Saito, T., Maniwa, Y., 2016. J. Chem. Phys. 145, 064514.
Lee, S.H., Kim, D., Kim, S., Han, C.-S., 2011. Appl. Phys. Lett. 99, 104103.
Lee, B., Baek, Y., Lee, M., Hong Jeong, D., Lee, H., Yoon, J., Kim, Y.H., 2015. Nat. Commun. 6, 7109.
Lee, S.-H., Kim, H.-R., Lee, H., Lee, J., Lee, C.-H., Lee, J., Park, J., Lee, K.-H., 2018. Chem. Eng. Sci. 192, 655–664.
Liao, Y., Picot, P., Lainé, M., Brubach, J.-B., Roy, P., Thill, A., Le Caër, S., 2018. Nano Res. 11, 1–15.
Li, J., Gong, X., Lu, H., Li, D., Fang, H., Zhou, R., 2007. Proc. Natl. Acad. Sci. USA 104, 3687–3692.
Li, X.-P., Kong, G.-P., Zhang, X., He, G.-W., 2013. Appl. Phys. Lett. 103, 143117.
Li, X., Yang, K., Su, J., Guo, H., 2014. RSC Adv. 4, 3245–3252.
Li, J., Li, W., Fang, H., Zhang, J., 2016. J. Phys. Chem. C 120, 6493–6501.
Liu, Y., Wang, Q., 2005. Phys. Rev. B 72, 085420.
Liu, Y., Wang, Q., Zhang, L., Wu, T., 2005. Langmuir 21, 12025–12030.
Liu, J., Dai, L., Baur, J.W., 2007. J. Appl. Phys. 101, 064312.

Liu, L., Qiao, Y., Chen, X., 2008. Appl. Phys. Lett. 92, 101927.
Liu, Y.-C., Shen, J.-W., Gubbins, K.E., Moore, J.D., Wu, T., Wang, Q., 2008. Phys. Rev. B 77, 125438.
Liu, K.-H., Zhang, Y., Lee, J.-J., Chen, C.-C., Yeh, Y.-Q., Chen, S.-H., Mou, C.-Y., 2013. J. Chem. Phys. 139, 064502.
Liu, B., Liu, J., Tu, X., Zhang, J., Zheng, M., Zhou, C., 2013. Nano Lett. 13, 4416–4421.
Lobo, A.O., Ramos, S.C., Antunes, E.F., Marciano, F.R., Trava-Airoldi, V.J., Corat, E.J., 2012. Mater. Lett. 70, 89–93.
Machado, F.M., Carmalin, S.A., Lima, E.C., Dias, S.L.P., Prola, L.D.T., Saucier, C., Jauris, I. M., Zanella, I., Fagan, S.B., 2016. J. Phys. Chem. C 120, 18296–18306.
Maillet, P., Levard, C., Spalla, O., Masion, A., Rose, J., Thill, A., 2011. Phys. Chem. Chem. Phys. 13, 2682–2689.
Majumder, M., Corry, B., 2011. Chem. Commun. 47, 7683–7685.
Majumder, M., Chopra, N., Andrews, R., Hinds, B.J., 2005. Nature 438, 44.
Majumder, M., Keis, K., Zhan, X., Meadows, C., Cole, J., Hinds, B.J., 2008. J. Membr. Sci. 316, 89–96.
Maniwa, Y., Kataura, H., Abe, M., Udaka, A., Suzuki, S., Achiba, Y., Kira, H., Matsuda, K., Kadowaki, H., Okabe, Y., 2005. Chem. Phys. Lett. 401, 534–538.
Maniwa, Y., Matsuda, K., Kyakuno, H., Ogasawara, S., Hibi, T., Kadowaki, H., Suzuki, S., Achiba, Y., Kataura, H., 2007. Nat. Materials 6, 135–141.
Matos, C.F., Galembeck, F., Zarbin, A.J.G., 2012. Carbon 50, 4685–4695.
Mattia, D., Calabrò, F., 2012. Microfluid. Nanofluid. 13, 125–130.
Mauter, M.S., Elimelech, M., 2008. Environ. Sci. Technol. 42, 5843–5859.
Melillo, M., Zhu, F., Snyder, M.A., Mittal, J., 2011. J. Phys. Chem. Lett. 2, 2978–2983.
Mendonça, B.H.S., de Freitas, D.N., Köhler, M.H., Batista, R.J.C., Barbosa, M.C., de Oliveira, A.B., 2019. Phys. A 517, 491–498.
Merz, P.T., Shirts, M.R., 2018. PLoS One 13, e0202764.
Michaelides, A., 2016. Nature 537, 171–172.
Misra, A., Giri, J., Daraio, C., 2009. ACS Nano 3, 3903–3908.
Miyauchi, M., Tokudome, H., 2007. J. Mater. Chem. 17, 2095–2100.
Mochizuki, K., Koga, K., 2015. Proc. Natl. Acad. Sci. USA 112, 8221–8226.
Moskowitz, I., Snyder, M.A., Mittal, J., 2014. J. Chem. Phys. 141, 18C532.
Mukherjee, S., Kim, K., Nair, S., 2007. J. Am. Chem. Soc. 129, 6820–6826.
Naguib, N., Ye, H., Gogotsi, Y., Yazicioglu, A.G., Megaridis, C.M., Yoshimura, M., 2004. Nano Lett. 4, 2237–2243.
Nomura, K., Kaneko, T., Bai, J., Francisco, J.S., Yasuoka, K., Zeng, X.C., 2017. Proc. Natl. Acad. Sci. USA 114, 4066–4071.
Noon, W.H., Ausman, K.D., Smalley, R.E., Ma, J., 2002. Chem. Phys. Lett. 355, 445–448.
Noy, A., Gyu Park, H., Fornasiero, F., Holt, J.K., Grigoropoulos, C.P., Bakajin, O., 2007. Nano Today 2, 22–29.
Ohba, T., 2014. Angew. Chem. 126, 8170–8174.
Ohba, T., Yamamoto, S., Kodaira, T., Hata, K., 2015. Langmuir 31, 1058–1063.
Oytun, F., Dizman, C., Karatepe, N., Alpturk, O., Basarir, F., 2017. Thin Solid Films 625, 168–176.
Palmer, J.C., Martelli, F., Liu, Y., Car, R., Panagiotopoulos, A.Z., Debenedetti, P.G., 2014. Nature 510, 385–388.
Park, M.J., Lee, J.K., Lee, B.S., Lee, Y.-W., Choi, I.S., Lee, S.-G., 2006. Chem. Mater. 18, 1546–1551.
Pascal, T.A., Goddard, W.A., Jung, Y., 2011. Proc. Natl. Acad. Sci. USA 108, 11794–11798.
Patel, A.J., Varilly, P., Jamadagni, S.N., Hagan, M.F., Chandler, D., Garde, S., 2012. J. Phys. Chem. B 116, 2498–2503.
Peng Lee, K., Leese, H., Mattia, D., 2012. Nanoscale 4, 2621–2627.
Perebeinos, V., Tersoff, J., 2014. Nano Lett. 14, 4376–4380.
Porada, S., Weinstein, L., Dash, R., van der Wal, A., Bryjak, M., Gogotsi, Y., Biesheuvel, P.M., 2012. ACS Appl. Mater. Interfaces 4, 1194–1199.
Pugliese, P., Conde, M.M., Rovere, M., Gallo, P., 2017. J. Phys. Chem. B 121, 10371–10381.
Qu, L., Dai, L., Osawa, E., 2006. J. Am. Chem. Soc 128, 5523–5532.
Ramazani, F., Ebrahimi, F., 2016. J. Phys. Chem. C 120, 12871–12878.
Roy, D., Tiwari, N., Gupta, M., Mukhopadhyay, K., Saxena, A.K., 2015. J. Phys. Chem. C 119, 716–723.
Sanchez-Valencia, J.R., Dienel, T., Gröning, O., Shorubalko, I., Mueller, A., Jansen, M., Amsharov, K., Ruffieux, P., Fasel, R., 2014. Nature 512, 61–64.
Scatena, L.F., Brown, M.G., Richmond, G.L., 2001. Science 292, 908–912.
Schäffel, D., Koynov, K., Vollmer, D., Butt, H., Schönecker, C., 2016. Phys. Rev. Lett. 116, 134501.
Schoch, R.B., Han, J., Renaud, P., 2008. Rev. Mod. Phys. 80, 839–883.
Schweiger, M., Schaudig, M., Gannott, F., Killian, M.S., Bitzek, E., Schmuki, P., Zaumseil, J., 2015. Carbon 95, 452–459.
Secchi, E., Marbach, S., Nigues, A., Stein, D., Siria, A., Bocquet, L., 2016. Nature 537, 210–213.
Setaro, A., 2017. J. Phys.: Condens. Matter 29, 423003.
Shayeganfar, F., Beheshtian, J., Shahsavari, R., 2018. Langmuir 34, 11176–11187.
Shim, M., Wong Shi Kam, N., Chen, R.J., Li, Y., Dai, H., 2002. Nano Lett. 2, 285–288.
Shiomi, J., Kimura, T., Maruyama, S., 2007. J. Phys. Chem. C 111, 12188–12193.
Shtogun, Y.V., Woods, L.M., 2009. J. Phys. Chem. C 113, 4792–4796.
Siria, A., Poncharal, P., Biance, A.-L., Fulcrand, R., Blase, X., Purcell, S.T., Bocquet, L., 2013. Nature 458, 455–458.
Smallenburg, F., Filion, L., Sciortino, F., 2014. Nat. Phys. 10, 653–657.
Sotthewes, K., Bampoulis, P., Zandvliet, H.J.W., Lohse, D., Poelsema, B., 2017. ACS Nano 11, 12723–12731.
Strano, M.S., Dyke, C.A., Usrey, M.L., Barone, P.W., Allen, M.J., Shan, H., Kittrell, C., Hauge, R.H., Tour, J.M., Smalley, R.E., 2003. Science 301, 1519–1521.
Striolo, A., 2007. Nanotechnology 18, 475704.
Striolo, A., Michaelides, A., Joly, L., 2016. Annu. Rev. Chem. Biomol. Eng. 7, 533–556.
Su, J., Guo, H., 2011. ACS Nano 5, 351–359.
Suk, M.E., Raghunathan, A.V., Aluru, N.R., 2008. Appl. Phys. Lett. 92, 133120.
Takaiwa, D., Hatano, I., Koga, K., Tanaka, H., 2008. Proc. Natl. Acad. Sci. USA 105, 39–43.
Tanaka, H., Koga, K., 2005. J. Chem. Phys. 123, 094706.
Tao, J., Song, X., Zhao, T., Zhao, S., Liu, H., 2018. Chem. Eng. Sci. 192, 1252–1259.
Tarjus, G., 1995. J. Chem. Phys. 103, 3071.
Ternes, P., Salcedo, E., Barbosa, M.C., 2018. Phys. Rev. E 97, 033104–033112.
Thomas, M., Corry, B., 2015. Philos. Trans. Roy. Soc. A 374, 2060.
Thomas, J.A., McGaughey, A.J.H., 2009. Phys. Rev. Lett. 102, 184502.
Thomas, M., Corry, B., Hilder, T.A., 2014. Small 10, 1453–1465.
Vaitheeswaran, S., Rasaiah, J.C., Hummer, G., 2004. J. Chem. Phys. 121, 7955–7965.
Vuković, L., Vokac, E., Král, P., 2014. J. Phys. Chem. Lett. 5, 2131–2137.
Waghe, A., Rasaiah, J.C., Hummer, G., 2002. J. Chem. Phys. 117, 10789–10795.
Wang, H.-J., Xi, X.-K., Kleinhammes, A., Wu, Y., 2008. Science 322, 80–83.
Wang, J., Liu, J., Yang, H., Chen, Z., Lin, J., Shen, Z.X., 2016. J. Mater. Chem. A 4, 7565–7572.
Wei, X., Luo, T., 2018. J. Phys. Chem. C 122, 5131–5140.
Wei, X., Tang, D.-M., Chen, Q., Bando, Y., Golberg, D., 2013. ACS Nano 7, 3491–3497.
Won, C.Y., Aluru, N.R., 2008. J. Phys. Chem. C 112, 1812–1818.
Wong-ekkabut, J., Karttunen, M., 2016. Biochim. Biophys. Acta Biomembr. 1858, 2529–2538.
Wu, K., Chen, Z., Li, J., Li, X., Xu, Jinze, Dong, X., 2017. Proc. Natl. Acad. Sci. USA 114, 3358–3363.
Xie, L., Shi, C., Cui, X., Zeng, H., 2017. Langmuir 33, 3911–3925.
Xu, B., Li, Y., Park, T., Chen, X., 2011. J. Chem. Phys. 135, 144703.
Xu, Y., Tian, X., Lv, M., Deng, M., He, B., Xiu, P., Tu, Y., Zheng, Y., 2016. J. Phys. D: Appl. Phys. 49, 285302.
Yang, H.Y., Han, Z.J., Yu, S.F., Pey, K.L., Ostrikov, K., Karnik, R., 2013. Nat. Commun. 4, 2220.
Yao, M., Wang, Z., Liu, B., Zou, Y., Yu, S., Lin, W., Hou, Y., Pan, S., Jin, M., Zou, B., Cui, T., Zou, G., Sundqvist, B., 2008. Phys. Rev. B 78, 205411.
Yesilbas, M., Boily, J.-F., 2016. J. Phys. Chem. Lett. 7, 2849–2855.
Yesilbas, M., Holmboe, M., Boily, J.-F., 2018. ACS Earth Space Chem. 2, 38–47.
Yuet, P.K., Blankschtein, D., 2010. J. Phys. Chem. B 114, 13786–13795.
Zang, J., Konduri, S., Nair, S., Sholl, D.S., 2009. ACS Nano 3, 1548–1556.
Zhang, M., Su, L., Mao, L., 2006. Carbon 44, 276–283.
Zhang, L., Li, J., Peng, G., Liang, L., Kong, Z., Shen, J.-W., Jia, L., Wang, X., Zhang, W., 2018. J. Mol. Liq. 258, 98–105.
Zhou, M., Hu, Y., Liu, J.-C., Cheng, K., Jia, G.-Z., 2017. Chem. Phys. Lett. 686, 173–177.
Zuo, G., Shen, R., Ma, S., Guo, W., 2010. ACS Nano 4, 205–210.